# Electronic Supplementary Information

# Epitaxial Coordination Assembly of a Semi-conductive Silver-chalcogenide Layer-based MOF

Chun-Hua Gong,[‡a] Xiao-Zong Hu,[‡a] Zhen Han,[a] Xiao-Fei Liu,[a] Min-Zi Yang[a] and Shuang-Quan Zang[*a]

[a] Henan Key Laboratory of Crystalline Molecular Functional Materials, Henan International Joint Laboratory of Tumor Theranostical Cluster Materials, Green Catalysis Center, and College of Chemistry, Zhengzhou University, Zhengzhou 450001, China,

* E-mail: zangsqzg@zzu.edu.cn

‡ The authors contributed equally.

## Materials and Methods

### Materials and reagents

Chemical reagents were purchased commercially and were used without further purification. $[^{i}PrSAg]_n$ precursor were synthesized from the reaction of molar equivalents of $AgNO_3$ and $^{i}PrSH$ in $Et_3N$. $CF_3COOAg$ precursor was prepared by the reaction of molar equivalents of $Ag_2O$ and $CF_3COOH$. N,N,N',N'-tetramethylethylenediamine can be abbreviated as TEMED, 1,2,4,5-benzenetetracarboxylic acid can be abbreviated as $H_4BTEC$. All solvents were analytical grade reagent.

### Preparation of complex 1 and complex 2

Synthesis of $[Ag_4(^{i}PrS)_3(CF_3COO)]_n$ (complex **1**). A mixture of $CF_3COOAg$ (0.1 mmol, 22 mg) and $[^{i}PrSAg]_n$ (0.05 mmol, 9.2 mg) was dissolved in 5 mL DMF/$^{i}$PrOH (V : V = 1 : 4) to obtain a clear solution at room temperature. Then 70 µL TEMED was added into the above solution. The resultant solution was sealed into 25 mL Teflon-lined autoclaves and heated at 60 °C for 24 hours. After cooling to room temperature, colorless elongated sheet crystals were obtained with a yield of 40% (based on $[^{i}PrSAg]_n$). Elemental analysis for complex **1** (calculated): C, 17.16% and H, 2.75%; (found): C, 17.17%; H, 2.69%.

Synthesis of $[Ag_6(^{i}PrS)_4(BTEC)_{0.5}]_n$ (complex **2**). Method **A**: A mixture of complex **1** (10 mg) and $H_4BTEC$ (0.05 mmol, 12.7 mg) was placed in 4 mL MeCN / EtOH (V : V = 1 : 1), then the solution was sealed into 25 mL Teflon-lined autoclaves and heated at 120 °C for 24 hours. After cooling to room temperature, colorless block crystals were obtained with a yield of 80% (based on complex 1). Method **B**: A mixture of $AgNO_3$ (0.1 mmol, 17 mg), $[^{i}PrSAg]_n$ (0.05 mmol, 9.2 mg), and $H_4BTEC$ (0.05 mmol, 12.7 mg) was dissolved in 4 mL MeCN / EtOH (V : V = 1 : 1) to obtain a clear solution at room temperature. Then the solution was sealed into 25 mL Teflon-lined autoclaves and heated at 60 °C for 24 hours. After cooling to room temperature, colorless block crystals were obtained with a yield of 35% (based on $[^{i}PrSAg]_n$). Elemental analysis for complex **2** (calculated): C, 19.03%; H, 2.72%; (found): C, 19.11%; H, 2.64%.

### Crystallographic data collection and refinement of the structure

Single-crystal X-ray diffraction measurement of complex **1** and complex **2** were performed on a Rigaku XtaLAB Pro diffractometer at 200 K with Mo-Kα radiation (λ = 0.73173 Å). Data collection and reduction were performed using the program CrysAlisPro.[1] All the structures were solved with direct methods (SHELXS)[2] and refined by full-matrix least squares on $F^2$ using *OLEX*[2],[3] which utilizes the SHELXL-2015 module.[4] All the atoms were refined anisotropically. Hydrogen atoms were placed in calculated positions refined using idealized geometries and assigned fixed isotropic displacement parameters. The crystal structures are visualized by *DIAMOND 3.2*. The detailed information of the crystal data, data collection and refinement results for MOFs are summarized in Table S1.

### Characterization

Infrared spectra were obtained using in the range of 4000-400 $cm^{-1}$. Thermogravimetric (TG) analyses were performed on a SDT 2960 thermal analyzer from room temperature to 500 °C at a

heating rate of 10 °C/min under nitrogen atmosphere. PXRD patterns of the complexes were collected at room temperature in air on an X'Pert PRO diffractometer (Cu-Kα). A Perkin–Elmer Model Lambda 750 UV–vis spectrometer was used to collect diffuse reflection spectra (DRS). Finely powdered MOF was used as a sample and $BaSO_4$ as a reference to obtain DRS spectra. Scanning electron microscope (SEM) images and energy dispersive spectrometer (EDS) mapping images were acquired using a Zeiss Sigma 500 emission scanning electron microscope with an accelerating voltage of 2–10 kV for SEM images and 20 kV for EDS mapping images.

## Second harmonic generation (SHG) measurements of complex 1

The SHG was tested via the Raman system (WITec alpha 300RS+) with a 40× objective. The attenuated laser (commercial Ti : Sapphire femtosecond laser, 140 fs 80 MHz) was used as the light source. The laser was focused on the sample and SHG signal was back collected using the Raman system. The angle-resolved polarized SHG was collected under parallel configuration (the polarized direction of incident laser is parallel to the direction of the single detector) and the sample was rotated 360° with a step of 20°.

## Electrical measurement and fabrication of single crystal electrode

The electronic measurement was realized by a semiconductor analyzer (B1500A, Keysight), and the electrode device is in a probe station (CGO-4, Cindbest) with HT-400 Thermostat. The single-crystal electrodes were made using SPI conductive silver paint (SPI 05002-AB) by placing the crystal between two electrodes. The sizes of the crystals are measured by a RX50M metalloscope.

## Luminescence measurements

Luminescence measurements were carried out using a HORIBA FluoroLog-3 fluorescence spectrometer. Variable-temperature steady-state emission spectra of solid-state complex **2** were performed using an East Changing TC202 temperature controller after each sample was evacuated for 30 min using a VALUE VRD-16 vacuum pump. Luminescence microscopy images were recorded on an Olympus BX53 microscope. Luminescence lifetime was measured on an Edinburgh FLS 1000 fluorescence spectrometer equipped with a 355 nm laser operating in time-correlated single-photon counting mode (TCSPC) with a resolution time of 340 μs. The photoluminescence quantum efficiency in powder form was measured using an integrating sphere with excitation at 371 nm on an Edinburgh FLS 1000 fluorescence spectrometer.

## Density functional theory (DFT) calculation

All the calculations was performed within the framework of the density functional theory (DFT) as implemented in the Vienna Ab initio Software Package (VASP 5.3.5) code within the Perdew-Burke-Ernzerhof (PBE) generalized gradient approximation and the projected augmented wave (PAW) method.[5] The cut-off energy for the plane-wave basis set was set to 450 eV. The Brillouin zone of the surface unit cell was sampled by Monkhorst–Pack (MP) grids, with k-point mesh for the surface optimizations of complex **1** and complex **2**.[6] Complex **1** and complex **2** were determined by 2 × 2 × 2 Monkhorst-Pack grid. The convergence criterion for the electronic self-consistent iteration and force was set to $10^{-7}$ eV and 0.01 eV/Å, respectively.

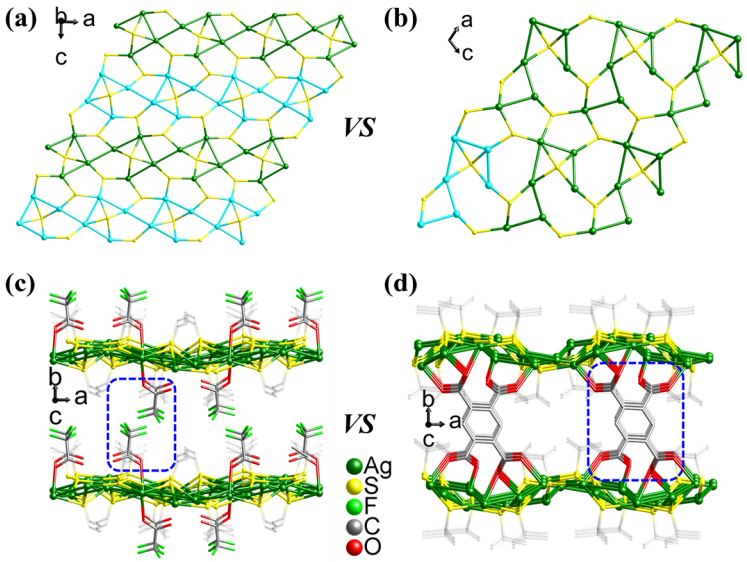


**Fig. S1** (a, c) Ag-S two-dimensional arrangement and packing structure of complex **1**. (b, d) Ag-S two-dimensional arrangement and three-dimensional structure of complex **2**.

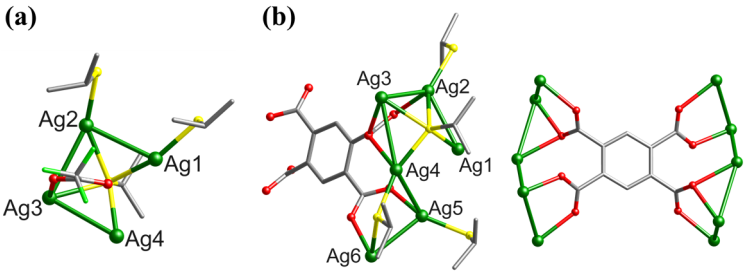


**Fig. S2** (a) Coordination environment of Ag ions in complex **1**. (b) Coordination environment of Ag ions and BTEC linker in complex **2**.

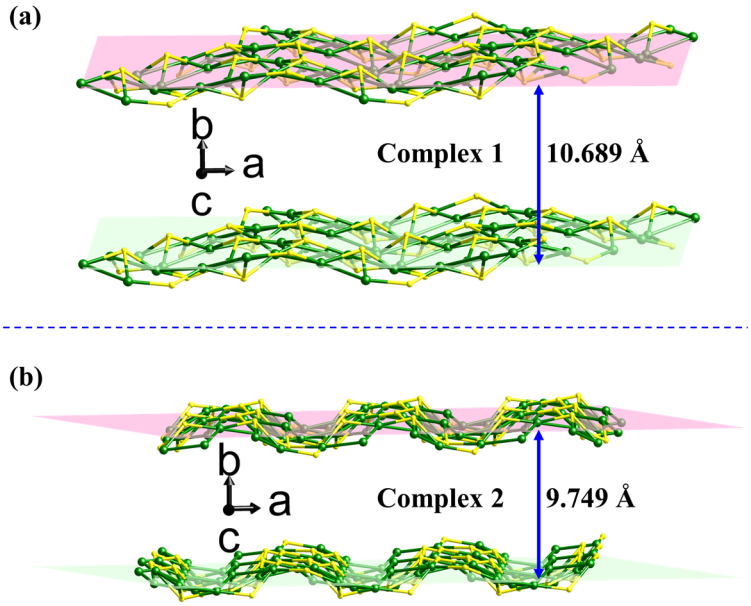


**Fig. S3** Distance between the adjacent Ag-S layers in complex **1** (a) and complex **2** (b).

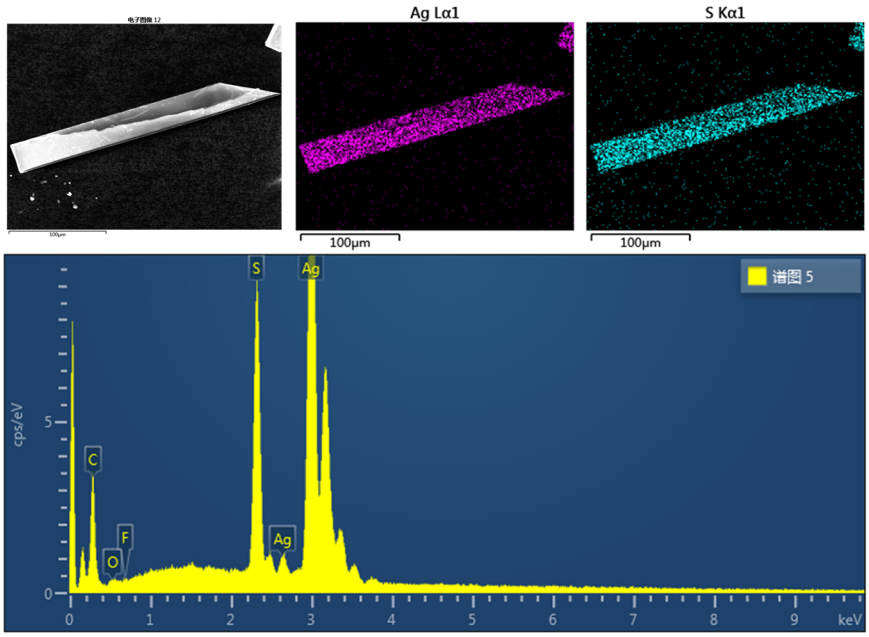


**Fig. S4** Morphology, elemental mapping and EDS measurement of complex **1**.

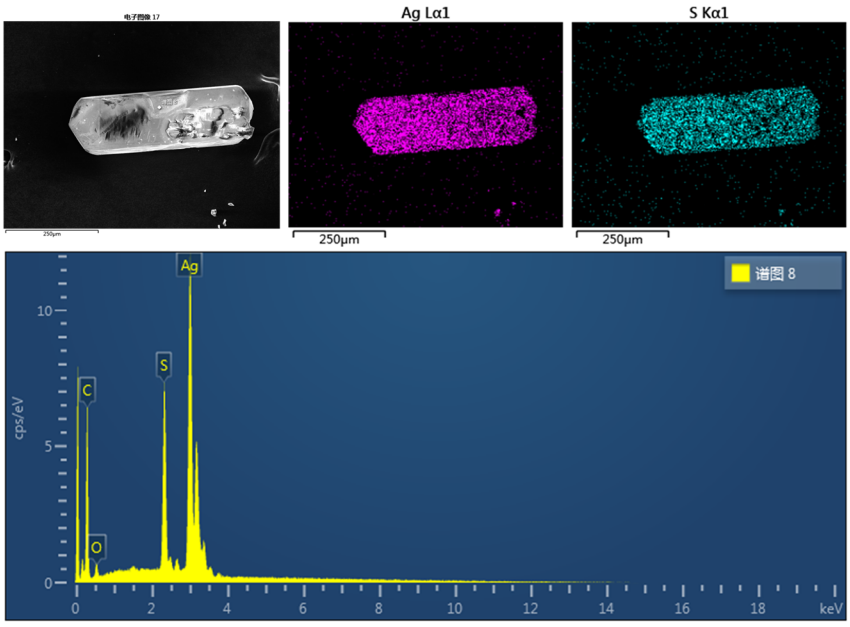


**Fig. S5** Morphology, elemental mapping and EDS measurement of complex **2**.

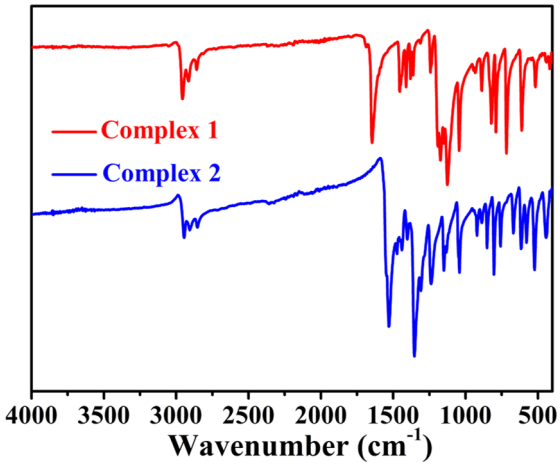


**Fig. S6** FT-IR spectra of complex **1** and complex **2**.

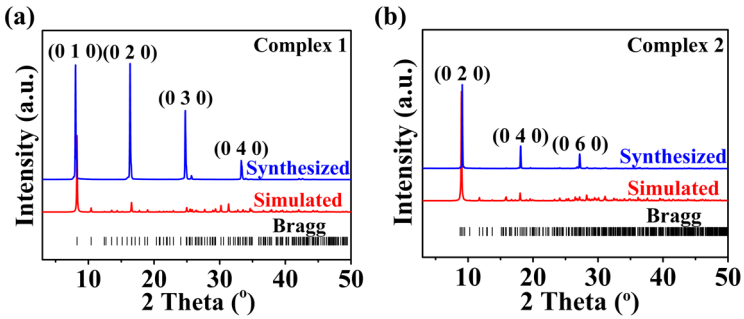


**Fig. S7** PXRD patterns of complex **1** (a) and complex **2** (b).

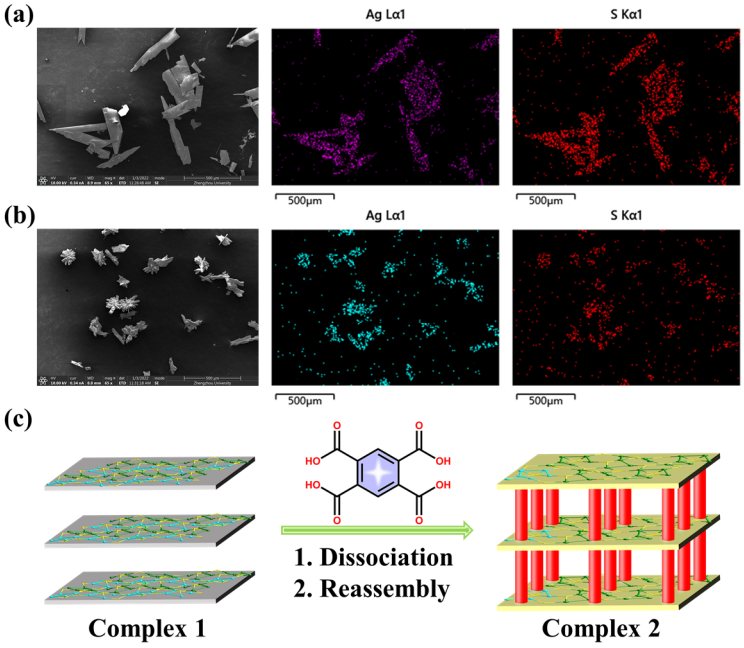


**Fig. S8** (a) Morphology, elemental mapping of complex **1** as starting materials in stepwise synthesis process. (b) Morphology, elemental mapping of complex **2** as target products in stepwise synthesis process. (c) The possible routes of the stepwise synthesis strategy.

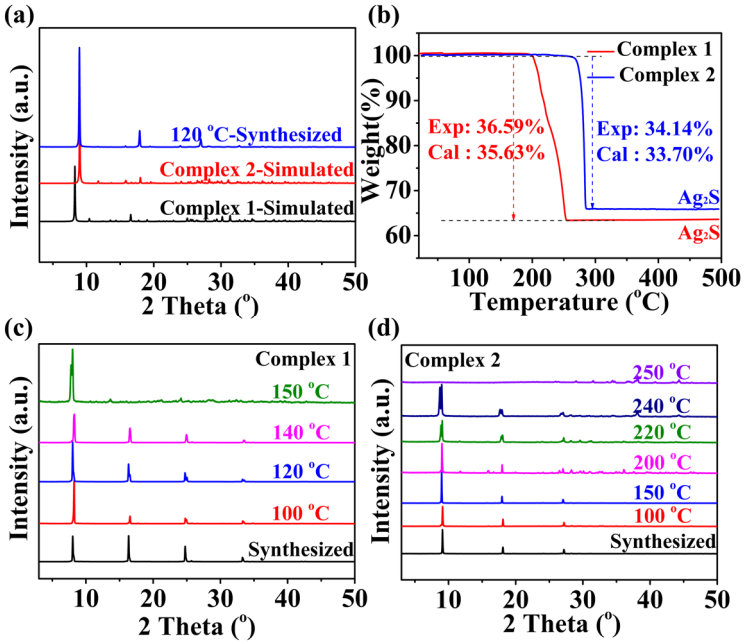


**Fig. S9** (a) PXRD patterns of complex **2** synthesized by complex **1** as starting materials. (b) Thermogravimetric curves of complex **1** and complex **2** under $N_2$ atmosphere. (c) Variable-temperature PXRD patterns of complex **1**. (d) Variable-temperature PXRD patterns of complex **2**.

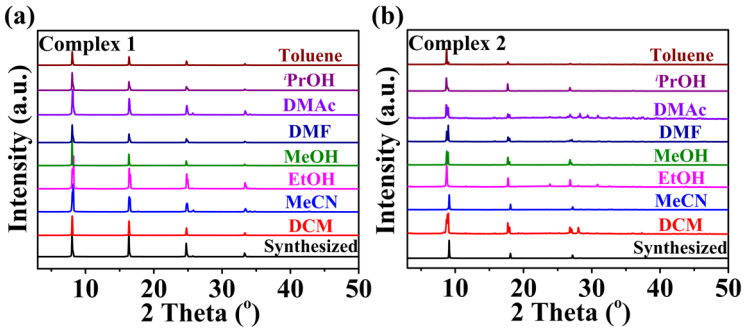


**Fig. S10** PXRD patterns of complex **1** (a) and complex **2** (b) after soaking in various organic solvents for 24 h.

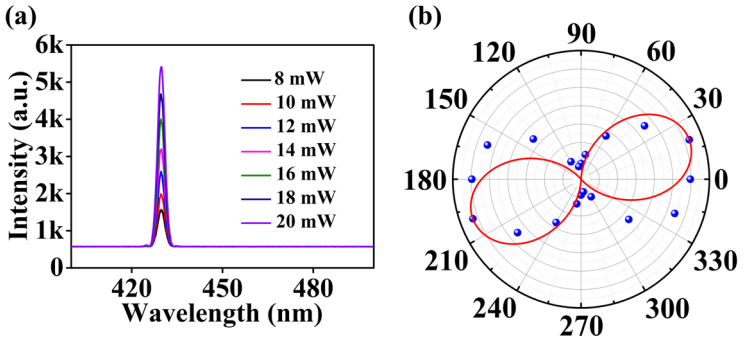


**Fig. S11** (a) SHG intensity change under different excitation power densities for complex **1**. (b) Polarization-angle-dependent SHG intensity for complex **1**.

Since complex **1** is crystallized in non-centrosymmetric space group, which should lead to nonlinear optical properties, so the single-crystal SHG was measured. In the Fig. S11a, the peaks located at 430 nm was observed, which is certainly SHG signals. At the wavelength of $\lambda_{ex}$ = 860 nm, when the excitation power of the incident laser is changed, the SHG intensity increases with the increase of the excitation power. Fig. S11b shows the SHG polarization dependence for complex **1**, where SHG intensity is plotted as a function of sample rotation angle. A clear dumbbell petal can be observed, which is consistent with the 2-fold structure symmetry of complex **1**. The angle dependence fitting formula can be described as $I = I_0 \sin^2(3\theta)$, where I and $I_0$ are the detected intensity and the maximum SHG intensity, respectively. SHG measurements reveal that complex **1** exhibits an obviously SHG response, which further proves its noncentrosymmetric crystal structure.

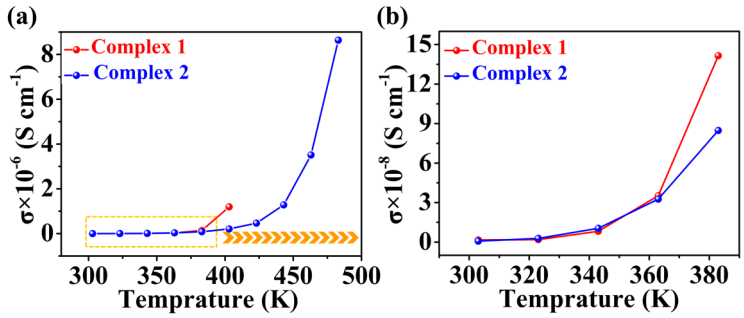


**Fig. S12** Temperature dependence of the electrical conductivity of complex **1** and complex **2**.

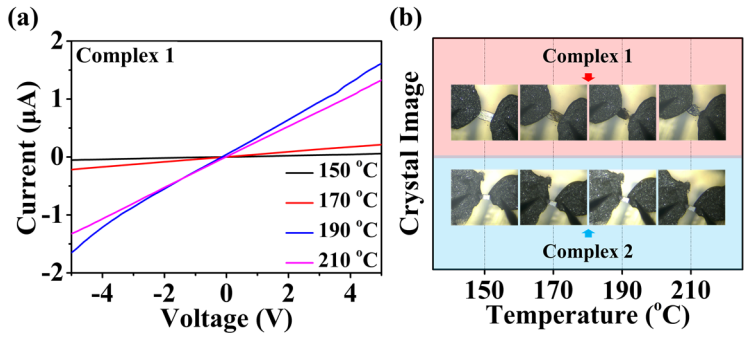


**Fig. S13** (a) The I–V curves of complex **1** at 150 °C 170 °C, 190 °C and 210 °C, respectively. (b) Photographs of the single crystals of complex **1** and complex **2** for electrical measurement at 150 °C, 170 °C, 190 °C and 210 °C, respectively.

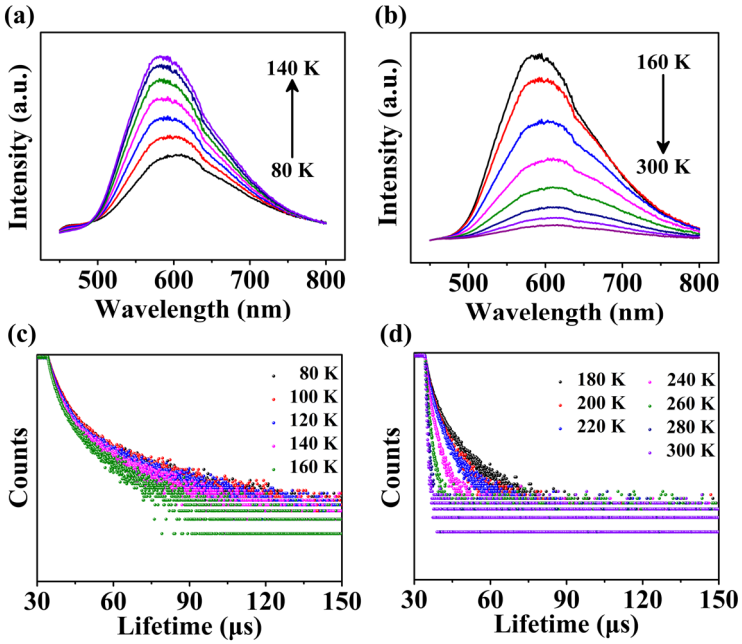


**Fig. S14** (a, b) Variable-temperature emission spectra of complex **2** from 80 K to 300 K. (c, d) Temperature dependence of the excited-state lifetimes of complex **2** in the range of 80 K to 300 K.

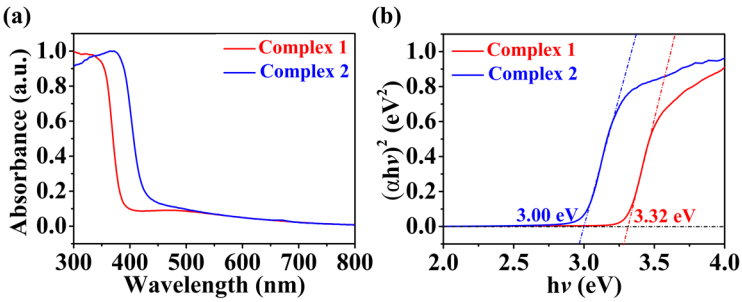


**Fig. S15** (a) UV-Vis diffuse reflectance spectra of complex **1** and complex **2** at room-temperature. (b) Tauc plot displaying the band gap of complex **1** and complex **2**.

The bandgap for complex **1** and complex **2** were calculated by means of the Tauc plot method and the equation for which is given as $(\alpha hv)^2 = A(hv - E_g)$ where $\alpha$ is the extinction coefficient, $h$ is the Planck's constant (J•s), $v$ is the light frequency ($s^{-1}$), $A$ is the absorption constant and $E_g$ is the band gap (eV). The indirect bandgap for the complex **1** and complex **2** was estimated by extrapolation to be 3.32 eV and 3.00 eV, respectively.

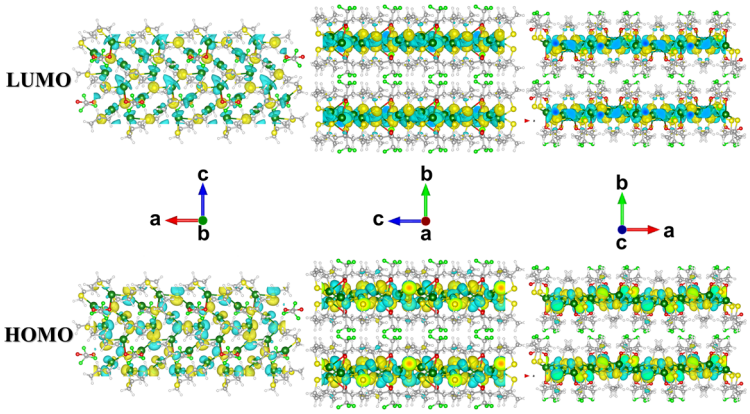


**Fig. S16** DFT calculation of HOMO and LUMO of complex **1** along different directions.

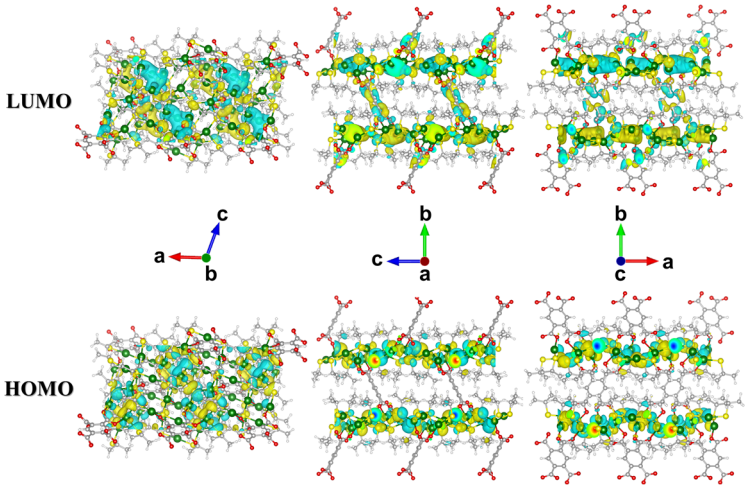


**Fig. S17** DFT calculation of HOMO and LUMO of complex **2** along different directions.

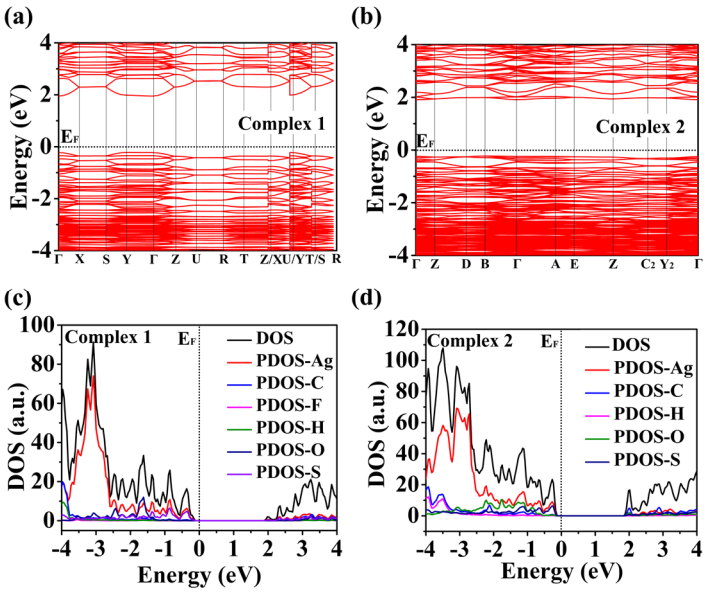


**Fig. S18** (a, b) Band structure of complex **1** and complex **2**. (c, d) The DOS (black line) and the PDOS (the colored lines) of complex **1** and complex **2**. The dashed black line at zero energy represents the Fermi level ($E_F$).

**Table S1** Crystal data and structure refinements for complex **1** and complex **2**.

| Identification code | **Complex 1** $[Ag_4(^iPrS)_3(CF_3COO)]_n$ | **Complex 2** $[Ag_6(^iPrS)_4(PA)_{0.5}]_n$ |
|---|---|---|
| CCDC number | 2112051 | 2112052 |
| Empirical formula | $C_{11}H_{21}Ag_4F_3O_2S_3$ | $C_{17}H_{29}Ag_6O_4S_4$ |
| Formula weight | 769.94 | 1072.86 |
| Temperature/K | 200.00(10) | 199.99(10) |
| Crystal system | orthorhombic | monoclinic |
| Space group | $Pca2_1$ | $P2_1/n$ |
| $a$/Å | 13.9132(6) | 11.2510(4) |
| $b$/Å | 10.6234(5) | 19.6897(6) |
| $c$/Å | 12.9987(7) | 12.4126(5) |
| $\alpha$/° | 90 | 90 |
| $\beta$/° | 90 | 109.191(4) |
| $\gamma$/° | 90 | 90 |
| Volume/Å$^3$ | 1921.28(16) | 2596.94(17) |
| $Z$ | 4 | 4 |
| $\rho_{calc}$ / g·cm$^{-3}$ | 2.662 | 2.744 |
| $\mu$/mm$^{-1}$ | 4.371 | 4.780 |
| $F$(000) | 1464 | 2036 |
| Radiation | MoKα (λ = 0.71073) | MoKα (λ = 0.71073) |
| 2Θ range for data collection/° | 3.834 to 58.37 | 4.044 to 58.318 |
| Index ranges | -17 ≤ h ≤ 18,<br>-13 ≤ k ≤ 14,<br>-17 ≤ l ≤ 15 | -13 ≤ h ≤ 15,<br>-26 ≤ k ≤ 24,<br>-15 ≤ l ≤ 15 |
| Reflections collected | 10488 | 23921 |
| Independent reflections | 3830 | 6039 |
| $R_{int}$ | 0.0423 | 0.0444 |
| $R_{sigma}$ | 0.0507 | 0.0424 |
| Data/restraints/parameters | 3830/1/214 | 6039/19/310 |
| Goodness-of-fit on F$^2$ | 1.198 | 0.965 |
| $R_1$[a], $wR_2$[b] [I>=2σ (I)] | 0.0317, 0.0851 | 0.0935, 0.2321 |
| $R_1$[a], $wR_2$[b] [all data] | 0.0427, 0.1192 | 0.1039, 0.2413 |
| Largest diff. peak/hole / e Å$^{-3}$ | 1.22/-1.65 | 1.82/-1.82 |
| Flack parameter | -0.04(7) | - |

[a] $R_1 = \sum||F_o| - |F_c||/\sum|F_o|$. [b] $wR_2 = \{\sum[w(F_o^2 - F_c^2)^2]/\sum[w(F_o^2)^2]\}^{1/2}$, $w = 1/[\sigma^2(F_o^2) + (0.1000P)^2]$ where $P = (F_o^2 + 2F_c^2)/3$.

**Table S2** Selected bond lengths (Å) for complex **1**.

| **Complex 1** | | | |
|---|---|---|---|
| Ag4−Ag3 | 3.1799(15) | Ag2−Ag1 | 3.0837(15) |
| Ag2−Ag3 | 3.2444(16) | Ag3−Ag1#2 | 3.1359(16) |
| Ag3−S1 | 2.574(3) | Ag1−S1 | 2.425(3) |
| Ag3−S3#3 | 2.447(3) | Ag1−S2 | 2.385(3) |
| Ag4−S1 | 2.653(3) | Ag2−S1 | 2.494(3) |
| Ag4−S3#1 | 2.570(3) | Ag2−S3 | 2.456(3) |
| Ag4−S2#1 | 2.467(3) | Ag2−S2#2 | 2.664(3) |
| Ag3−O1 | 2.344(10) | | |

Symmetry codes: #1 *3/2-x, +y, 1/2+z;* #2 *-1/2+x, 1-y, +z;* #3 *1-x, 1-y, 1/2+z;* #4 *1/2+x, 1-y, +z.*

**Table S3** Selected bond lengths (Å) for complex **2**.

| **Complex 2** | | | |
|---|---|---|---|
| Ag2−Ag3 | 2.917(2) | Ag6−Ag5 | 3.002(2) |
| Ag2−Ag1 | 2.999(2) | Ag5−Ag4 | 3.028(2) |
| Ag2−S1 | 2.412(4) | Ag6−S3 | 2.591(5) |
| Ag2−S2 | 2.560(5) | Ag6−O4 | 2.379(13) |
| Ag2−O1 | 2.333(13) | Ag5−S4 | 2.378(5) |
| Ag3−S4#1 | 2.509(5) | Ag5−O3 | 2.189(12) |
| Ag3−S1#2 | 2.532(4) | Ag4−S3 | 2.395(5) |
| Ag3−S2 | 2.633(5) | Ag4−S2 | 2.419(5) |
| Ag3−O2 | 2.443(12) | Ag4−O2 | 2.533(11) |
| Ag6−S4#2 | 2.621(4) | Ag1−S3#4 | 2.372(5) |
| Ag6−S1#3 | 2.484(5) | Ag1−S2 | 2.397(5) |

Symmetry codes: #1 *1/2+x, 1/2-y, -1/2+z; #2 -1/2+x, 1/2-y, -1/2+z;* #3 *-1+x, +y, +z;* #4 *1/2+x, 1/2-y, 1/2+z.*

## References


1 (a) CrysAlisPro, Version 1.171.36.31. Agilent Technologies Inc., Santa Clara, CA, USA 2012; (b) O. D. Rigaku, CrysAlisPro Software System, Version 1.171.38.41k, Rigaku Coorporation, Oxford, UK 2015.

2 G. M. Sheldrick, *Acta Cryst. A*, 2008, **64**, 112-122.

3 O. V. Dolomanov, L. J. Bourhis, R. J. Gildea, J. A. K. Howard and H. Puschmann, *J. Appl. Cryst.*, 2009, **42**, 339-341.

4 G. M. Sheldrick, *Acta Cryst. C*, 2015, **71**, 3-8.

5 (a) J. P. Perdew, K. Burke and M. Ernzerhof, *Phys. Rev. Lett.*, 1996, **77**, 3865-3868; (b) B. Hammer, L. B. Hansen and J. K. Nørskov, *Phys. Rev. B*, 1999, **59**, 7413-7421; (c) P. E. Blöchl, *Phys. Rev. B*, 1994, **50**, 17953-17979; (d) G. Kresse and D. Joubert, *Phys. Rev. B*, 1999, **59**, 1758-1775.

6 H. J. Monkhorst and J. D. Pack, *Phys. Rev. B*, 1976, **13**, 5188-5192.